Sensitivity analysis of the diffusion boundary layer steam condensation model

BIAN Haozhi[1], SUN Zhongning[1], ZHANG Nan[1], MENG Zhaoming[1], and DING Ming[1]

1. *Fundamental Science on Nuclear Safety and Simulation Technology Laboratory, Harbin Engineering University, Harbin, China, 150001 (bianhaozhi@yeah.net)*

Abstract: In loss of coolant accidents (LOCAs), steam condensation in the presence of air is of vital importance. This is due to the initial and long term containment residual heat removal are closely related to the condensation heat transfer efficiency. In related numerical analyses, the diffusion boundary layer condensation model has been developed for the containment thermal-hydraulic analysis. However, the sensitivity of this model to some influential factors has not been quantitatively evaluated. In the present work, by analyzing mechanisms of the condensation model, three factors were concluded to be influential on the steam condensation model. They are: the mass transfer caused by the large temperature gradient in the near wall region (Soret effect), the effect of various diffusion coefficients on the model accuracy (Diffusion coefficient effect) and the effect of the mass fraction gradient in the near wall region (wall treatment effect). The influence of these factors was evaluated delicately based on numerical analysis on the COPAIN facility. The results indicate that the Soret effect takes around 5% in the total mass transfer in the saturated group and can be more than 40% in the superheated group; the maximum relative difference among various diffusion coefficient equations is 26%, and the value varies with air mass fraction and wall sub-cooling; the automatic wall treatments can give reasonable predictions on condensation heat transfer performance, and the accuracy of different wall treatment methods various.

Keyword: CFD; steam condensation; non-condensable gas; condensation model; sensitivity analysis

1. Introduction

Steam condensation in the presence of air is an important heat transfer process in various engineering applications including the design of heat exchangers and the employment of the passive containment cooling system in the third generation nuclear power plants [1,2]. To investigate the influence of air on condensation heat transfer, various experimental and theoretical studies have been performed [1,3-5]. The experimental studies show that air has an obvious deterioration effect on condensation heat transfer, leading to its condensation heat transfer coefficient an order of magnitude smaller than that of the pure steam condensation. Theoretical analysis indicates that the main thermal resistance for steam condensation in the presence of air lies in the high concentration air layer in the near-wall region rather than the water film attached on the heat transfer surface [6-9]. These studies laid foundations for related research area and some conclusions have already been used in the nuclear safety systematic analysis.

Enlightened by the Fukushima nuclear accident and promoted by the fast growth of computational performance, there is an increasing demand in multi-dimensional simulations on containment thermal hydraulics. Amongst various related numerical models, steam condensation in the presence of air is the most important one. It directly affects the containment residual heat removal, and determines local field distributions. In the past few decades, two commonly used steam condensation models have been developed. One is the experimental correlation model, and the other is the diffusion boundary layer model [10].

The experimental correlation model is based on condensation heat transfer coefficient experimental correlations in terms of air mass fraction, pressure, wall sub-cooling *etc.*, and in calculations, the total condensation heat transfer is calculated by the Newton's law of cooling. The condensation rate is

Received date: April 21, 2018
(Revised date: June 21, 2018)

calculated by dividing the total heat transfer by the steam latent heat. However, this model is based on a certain experiment and only applicable within the experimental parameter range. There may have large error when it exceeds the experimental parameter scope. Moreover, this model is based on the global average parameters, so the diffusion of steam through the near-wall air layer may not be properly evaluated.

The diffusion boundary layer model is based on the diffusion theory or the Fick's law. This model can give reasonable predictions of steam condensation in most cases and considered the diffusion of steam through the near-wall high concentration air layer. Compared to the experimental correlation model, the diffusion boundary layer model possesses theoretical basis and demonstrates advantages in local phenomena analyses. Thus, it is generally applied in latest studies and considered to be promising the future containment thermal-hydraulic analysis. Nevertheless, there are still some concerns related to the model sensitivity and application scope. By analyzing the diffusion boundary layer model equations, three influential aspects are concluded. They are: the thermal diffusion effect or the Soret effect, diffusion coefficient effect, and the boundary concentration gradient effect (wall function effect). The detailed depictions of these three effects are as follows.

Firstly, in the mass transfer theory, the diffusion of steam in the steam-air mixture gas is mainly driven by two aspects. One is the concentration gradient in the near-wall region, and the other is the temperature gradient in this region. The mass transfer driven by the latter process is also regarded as the Soret effect. In most related numerical simulations, merely the concentration gradient induced mass transfer is considered. However, in some applications *e.g.* refineries in chemical industries and severe accidents in nuclear power plants, there may also exists large temperature gradient between the mainstream and liquid-gas interface [11,12]. In such circumstances, the influence of Soret effect on the total mass transfer should also be evaluated.

Secondly, in the evaluation of binary gas diffusion, various diffusion coefficient formulas have been proposed. Some of them are based on the molecular kinetic theory, some are semi-empirical correlation. In the previous literature, various diffusion coefficient equations have been used in the evaluation of steam condensation in the presence of air. Typically, the Gilliland equation [13], Fuller equation [14], kinetic theory equation [9,15], Marrero and Mason equation [11], equation quoted by Yadav [16] *etc*. However, the deviations among these diffusion coefficients were not discussed in detailed.

Thirdly, in the application of the diffusion boundary layer condensation model, refined boundary layer meshes are required, which means the computational cost can be considerable. The complex layout of containment inner structure may make the number of meshes even greater. This may set back the applicability of this model in containment thermal-hydraulic analysis. A potential answer for this concern is using the automatic wall treatment. This method could give a reasonable prediction in flow and heat transfer in both refined and coarse mesh conditions, and it has been generally applied in general simulations cases like single phase flow. However the applicability of this method in steam condensation calculations should be further discussed.

2. Numerical method

2.1 Governing equations and turbulence model

To evaluate the condensation model sensitivity to the three influential factors, the CFD code STAR-CCM+ was employed to solve the governing equations, turbulence models and diffusion boundary layer steam condensation model. The CFD code uses finite volume method to solve the conservation equations with three dimensional discrete meshes. The mass, species, momentum and energy conservation equations are as follows.

Mass conservation:

$$\frac{\partial \rho}{\partial t} + \nabla \cdot (\rho \mathbf{w}) = S_m \tag{1}$$

Momentum conservation:

$$\frac{\partial (\rho \mathbf{w})}{\partial t} + \nabla \cdot (\rho \mathbf{w}\mathbf{w}) = \nabla \cdot P + \rho f + S_{\rho v} \tag{2}$$

Energy conservation:

$$\frac{\partial(\rho E)}{\partial t}+\nabla\cdot(\rho \mathbf{w}E)=\rho f\cdot\mathbf{w}+\nabla\cdot(P\cdot\mathbf{w})+\nabla\cdot(k_{eff}\nabla T)+S_h \quad (3)$$

Species conservation:

$$\frac{\partial(\rho\omega_j)}{\partial t}+\nabla\cdot(\rho\mathbf{w}\omega_j)=\nabla\cdot(\rho D_j\nabla\omega_j)+S_{m,j} \quad (4)$$

In addition to the basic governing equations, turbulence models are also required to assess the turbulent kinetic energy and turbulent dissipation rate. The STAR-CCM+ code recommended realizable k-ε turbulence with two layers all y+ treatment was employed. The all Y+ wall treatment is a hybrid treatment that emulates the low-Y+ wall treatment for fine meshes and the high-Y+ wall treatment for coarse meshes. It is also formulated with the desirable characteristic of producing reasonable answers for meshes of intermediate resolution, that is, when the wall-cell centroid falls within the buffer region of the boundary layer. The governing equations of the Realizable k-ε turbulence model are as follows.

$$\frac{\partial(\rho k)}{\partial t}+\frac{\partial(\rho\mathbf{w}_j k)}{\partial x_j}=\frac{\partial}{\partial x_j}\left[(\mu+\frac{\mu_t}{\mathrm{Pr}_k})\frac{\partial k}{\partial x_j}\right]+P_k+G_b-\rho\varepsilon-Y_M \quad (5)$$

$$\frac{\partial(\rho\varepsilon)}{\partial t}+\frac{\partial(\rho\mathbf{w}_j\varepsilon)}{\partial x_j}=\frac{\partial}{\partial x_j}\left[(\mu+\frac{\mu_t}{\mathrm{Pr}_\varepsilon})\frac{\partial\varepsilon}{\partial x_j}\right]+\rho C_1\bar{S}\varepsilon-C_2\rho\frac{\varepsilon^2}{k+\sqrt{\nu\varepsilon}}+C_{\varepsilon1}\frac{\varepsilon}{k}C_{\varepsilon3}G_b \quad (5)$$

2.2. Condensation model

The original governing equations and turbulence models cannot directly evaluate steam condensation, so additional equations for steam condensation rate are required. In the diffusion boundary layer condensation model, the steam condensation rate is derived from the combination of steam and air mass transfer equations [17] and the final equation is:

$$m_{cond}=-(\frac{\rho D}{1-\omega_v})\frac{\partial\omega_v}{\partial n}\bigg|_i \quad (6)$$

The simulation of steam condensation is realized by proper treatments of the source terms in the governing equations. The source terms of mass, momentum and energy are:

Mass source term:

$$S_m=S_v=m_{cond}/\Delta=-(\frac{\rho_{g,i}D}{1-\omega_{v,i}})\frac{\partial\omega_v}{\partial n}\big|_i/\Delta \quad (7)$$

Where, the diffusion coefficient D was generally predicted by the empirical correlation proposed by Fuller [18]:

$$D=D_0(\frac{T}{T_0})^{1.75}(\frac{P}{P_0})^{-1} \quad (8)$$

Where T_0 is the standard state temperature of 298 K, P_0 is standard pressure of 0.1MPa, D_0 is the mass diffusion coefficient of 2.6×10^{-5} m^2/s.

Momentum source term:

$$S_{\rho w}=S_m w \quad (9)$$

Energy source term:

$$S_h=S_m h_v \quad (10)$$

3. Validation of the condensation model

Before evaluating the influencing factors, validations of the diffusion boundary layer steam condensation model were firstly performed based on the COPAIN experiment [19]. The COPAIN experiments were carried out to investigate the relationship between condensation heat transfer and influential parameters including pressure, temperature, gas velocity and air mass fraction. As shown in Fig. 1, the test facility mainly consists of a vertical rectangular channel with a cross section of 0.6 m by 0.5 m. A condensation plate is on one sidewall of the channel with an area of 0.6 m by 2.0 m. In order to validate the diffusion boundary layer model in a broad parameter range, six typical experimental cases were selected. In these cases, the flow conditions include natural convection, free convection and forced convection with velocities ranging from 0.1 m/s to 3 m/s.

To simulate the six experimental cases, proper boundary conditions were set on various surfaces. The top surface was set as velocity inlet with various gas components and temperatures, the bottom surface was set as pressure outlet, the condensation wall was set as a constant temperature boundary and other walls were considered in an adiabatic condition. To reduce computational costs, the symmetric simulation was applied. The detailed parameters for the COPAIN simulation cases are listed in Table 1.

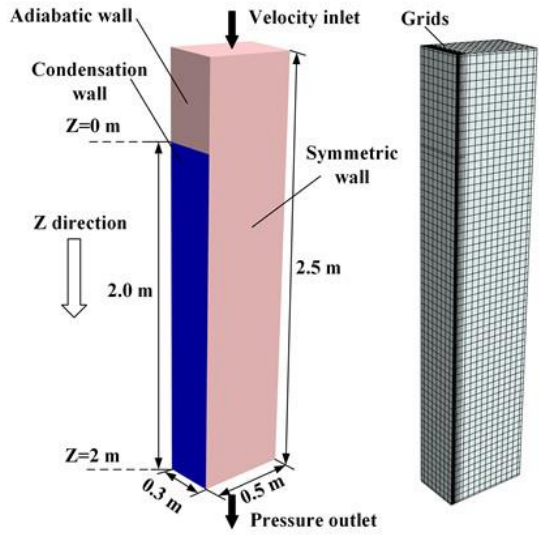

Fig. 1. Schematic diagram of COPAIN experiment.

Fig. 2 shows local heat flux comparisons between CFD calculated results and experimental data. It demonstrates that, in Z direction, the heat flux distributions predicted by numerical method generally agree well with the experimental data. Both results indicate that the heat flux has a large decrease in the initial region, then followed by a relatively flat heat flux distribution. By comparing the CFD results and the experimental ones at the measuring points, it illustrates that more than 93% numerical results are within 25% deviation of experimental data. Hence, the diffusion boundary layer model could give a reasonable prediction of condensation heat transfer property under various flow conditions.

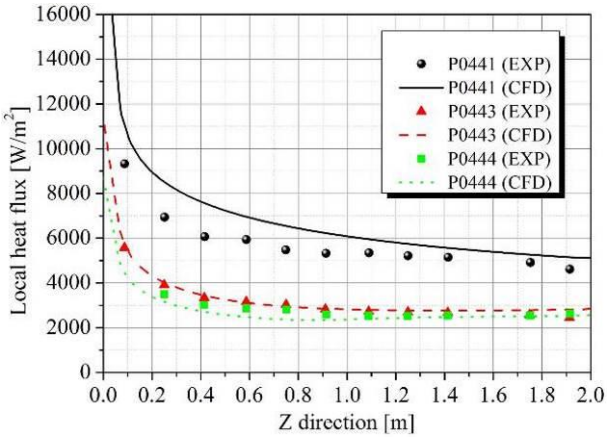

(a) Cases of P0441, P0443 and P0444

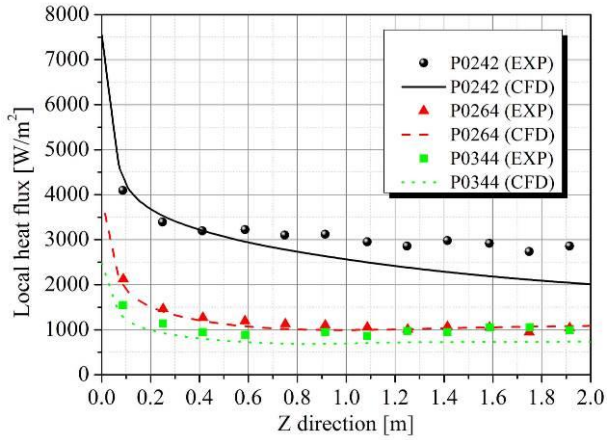

(b) Cases of P0242, P0264 and P0344

Fig. 2. Comparisons of local heat flux at different conditions.

Table 1. The test conditions for the COPAIN experiment

Test Number	Convective heat transfer	Inlet velocity (m/s	Pressure (bar)	Inlet temperature (K)	Wall Temperature (K)	Air mass fraction
P0441	Forced	3	1.02	353.23	307.4	0.767
P0443	Free	1	1.02	352.33	300.06	0.772
P0444	Natural	0.5	1.02	351.53	299.7	0.773
P0344	Natural	0.33	1.21	344.03	322	0.864
P0242	Forced	2	4.46	422.5	304.28	0.99
P0264	Natural	0.52	1.19	344.87	313.28	0.867

4. Sensitivity evaluations

4.1 The Soret effect

To analysis the Soret effect, both the concentration gradient induced mass transfer and the temperature gradient induced mass transfer are considered in the mass transfer equations as show in Eq. (11) and Eq. (12) [20-22]. A combination of these two equations is the total mass transfer at the liquid-gas interface (as shown in Eq. (13)). Considering only the steam component condensates at the liquid-gas interface, the sum of steam and air mass fraction equals a unit, and the sum of $D_{T,v}$ and $D_{T,air}$ equals zero [20], so the equation can be rewritten as Eq. (14).

$$m_v = \rho w \omega_v - \rho D \frac{\partial \omega_v}{\partial n} - \rho \frac{D_{T,v}}{T} \frac{\partial T}{\partial n} \quad (11)$$

$$m_{air} = \rho w \omega_{air} - \rho D \frac{\partial \omega_{air}}{\partial n} - \rho \frac{D_{T,air}}{T} \frac{\partial T}{\partial n} \quad (12)$$

$$m_v + m_{air} = \rho w \left(\omega_v + \omega_{air} \right) - \rho D \frac{\partial \left(\omega_v + \omega_{air} \right)}{\partial n}\bigg|_i - \rho \frac{\left(D_{T,v} + D_{T,air} \right)}{T} \frac{\partial T}{\partial n} \quad (13)$$

$$\rho w = m_v \quad (14)$$

Substituting Eq. (14) into Eq. (11), the final expression for the steam condensation rate is shown in Eq. (15). It is clear that the equation mainly contains two items on the right side which represents the concentration diffusion effect and the thermal diffusion effect (also the Soret effect) respectively. In these two terms, the diffusion property was represented by the binary diffusion coefficient D and the thermal diffusion coefficient D_T.

$$m_v = -\frac{\rho D}{\left(1-\omega_v\right)} \frac{\partial \omega_v}{\partial n}\bigg|_i + \left(\frac{1}{1-\omega_v} \right) \rho \frac{D_T}{T} \frac{\partial T}{\partial n} \quad (15)$$

The binary diffusion coefficient can be predicted by the Fuller model [18] (as given in Eq. (9)), and the thermal diffusion coefficient is usually predicted by the Warnatz model [23]. In the Warnatz model, the thermal diffusion coefficient is calculated by the thermal diffusion ratio K and the binary diffusion coefficient D as shown in Eq. (17), amongst which, the thermal diffusion ratio is predicted by the molecular kinetic theory as shown in Eq. (17) and Eq. (18)).

$$D_T = D\,K \quad (16)$$

Where

$$K = a X_v X_{air} \quad (17)$$

$$a = \frac{15}{2} \frac{\left(2A^*_{\mathrm{v,air}} + 5\right)\left(6C^*_{\mathrm{v,air}} - 5\right)}{A^*_{\mathrm{v,air}} \left(16A^*_{\mathrm{v,air}} - 12B^*_{\mathrm{v,air}} + 55\right)} \frac{M_v - M_{air}}{M_v + M_{air}} \quad (18)$$

Where, the three collision integral ratios are calculated by

$$A^*_{\mathrm{v,air}} = \frac{1}{2} \frac{\Omega^{(2,2)}_{\mathrm{v,air}}}{\Omega^{(1,1)}_{\mathrm{v,air}}} \quad (19)$$

$$B^*_{\mathrm{v,air}} = \frac{1}{3} \frac{5\Omega^{(1,2)}_{\mathrm{v,air}} - \Omega^{(1,3)}_{\mathrm{v,air}}}{\Omega^{(1,1)}_{\mathrm{v,air}}} \quad (20)$$

$$C^*_{\mathrm{v,air}} = \frac{1}{3} \frac{\Omega^{(1,2)}_{\mathrm{v,air}}}{\Omega^{(1,1)}_{\mathrm{v,air}}} \quad (21)$$

Where $\Omega_{v,\mathrm{air}}$ represents collision integrals between steam component and air component. It is a nonlinear function determining the variation of the distribution function resulting from pair collisions. Its value can be obtained by table lookup using reduced temperature and reduced dipole moment as follows[24].

$$T^*_{Steam,Air} = \frac{T_{Steam,Air}}{\varepsilon_{Steam,Air} / k_{Steam,Air}} \quad (22)$$

$$\delta_{steam,\,\mathrm{air}} = \frac{1}{4} \mu^{*2} \varsigma \left(\theta_1, \theta_2, \phi \right) \quad (23)$$

The evaluation of the Soret effect is based on the COPAIN experimental facility. Numerical results for three COPAIN experimental cases with various inlet velocities are shown in Fig. 3-5. In these figures, the concentration gradient induced mass transfer $m_{\mathrm{v,C}}$, the thermal gradient induced mass transfer $m_{\mathrm{v,T}}$, the total mass transfer $m_{\mathrm{v,C+T}}$ and the proportion of thermal gradient induced mass transfer in total mass transfer $m_{\mathrm{v,T}}$ /$m_{\mathrm{v,C+T}}$ are compared. The results demonstrate that all the three mass transfer rates decrease in Z direction. This can be explained by the condensation model expression together with the temperature and concentration gradient distribution in the near condensation wall region. In Eq.(15), it is clear that the concentration and temperature gradient are two main factors that affect the mass transfer character.

Fig. 6 indicates that the concentration and temperature gradient decreases along the condensation wall in the flow direction which facilitates the formation of the decreasing mass transfer distribution.

The velocities in these three experimental cases are 0.5 m/s, 1.0 m/s and 3.0 m/s respectively, and the wall sub-cooling is all around 50°C. The results show that the velocity has negligible effect on the thermal diffusion property and the proportion of the temperature gradient induced mass transfer in the total mass transfer is around 4%.

The temperature gradient induced mass transfer proportion of the six simulation cases are shown in Fig. 7. It is clear that the maximum values are close to the average ones. This is because both the concentration and temperature gradient induced mass transfer decreases along the condensation wall as shown in Fig. 3-5, which leads to a little change of the mass transfer ratio. Fig. 7 also indicates that the temperature gradient induced mass transfer generally takes a small proportion in the last five cases with a value around 5%. However, for the case P0242, the proportion is around 30%. This could be caused by two reasons. One is the large temperature difference between condensation wall and mainstream, the other is the large air mass fraction.

Table **1** indicates that the temperature gradient of case P0242 is 118.2℃, whereas the value in the other five cases is in the scope of 22.3~52.3℃. The large temperature gradient would enlarge the temperature gradient induced mass transfer. The air mass fraction in the case P0242 is 0.99 which is much larger than the other 5 cases. The large air mass fraction may to a large degree sets back the concentration gradient induced mass transfer, which in return increases the proportion of temperature gradient induced mass transfer.

To have an insight on this problem, several cases with various air mass fractions and temperature gradients are simulated. The simulations can be mainly divided into two groups. The first group maintains the mainstream steam at its saturation temperature, and the condensation wall temperature decreases in order to obtain various wall sub-cooling. Here, we define it as the saturation group. In the second group, the mainstream steam temperature is superheated and the degree of it ranges from 0 ℃ to 120℃. In the meanwhile, the wall sub-cooling is maintained at a constant. We define the second group as the superheated group.

In the saturation group, the air mass fraction ranges from 0.1 to 0.99 and the temperature gradient ranges from 20℃to 120℃. The numerical results are shown in Table 2. It is concluded that the proportion of temperature gradient induced mass transfer in the total mass transfer has a slight increase with the increase of temperature gradient and the air mass fraction. Generally, the proportion is less than 5%, which means the thermal diffusion effect could be neglected when the mainstream is at its saturation state.

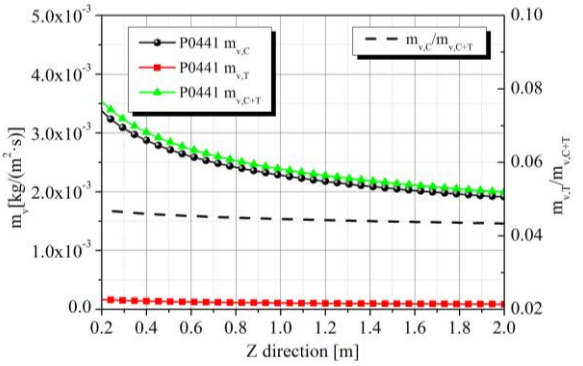

Fig. 3. Mass transfer rates and mass transfer ratio in P0441.

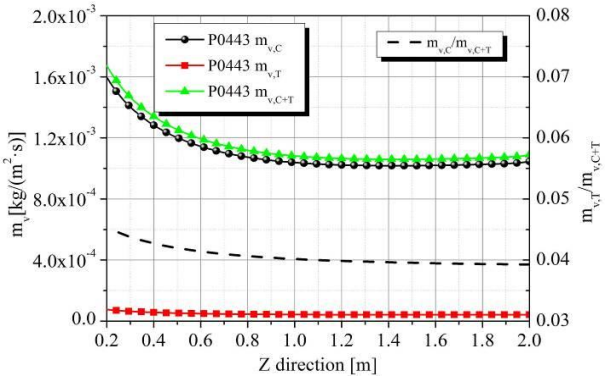

Fig. 4. Mass transfer rates and mass transfer ratio in P0443.

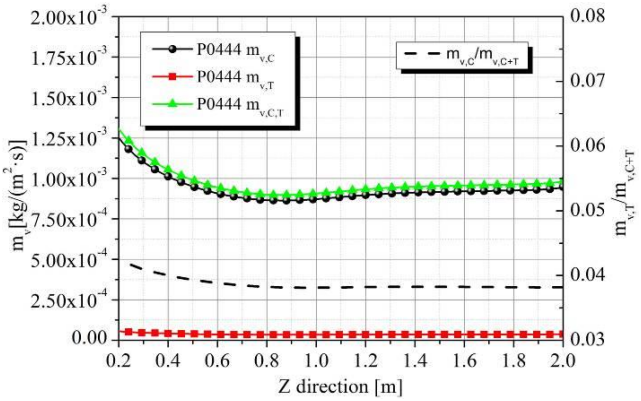

Fig. 5. Mass transfer rates and mass transfer ratio in P0444.

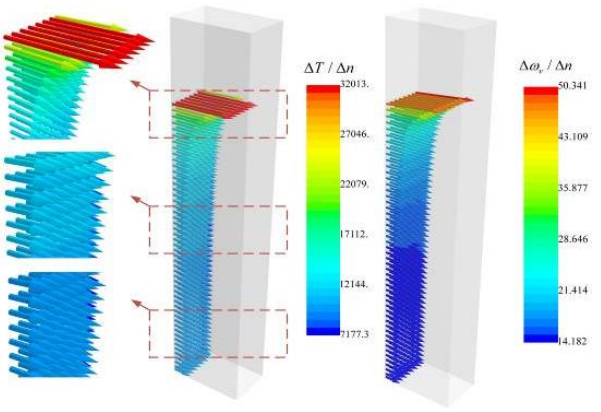

Fig. 6. Temperature gradient at condensation wall boundary.

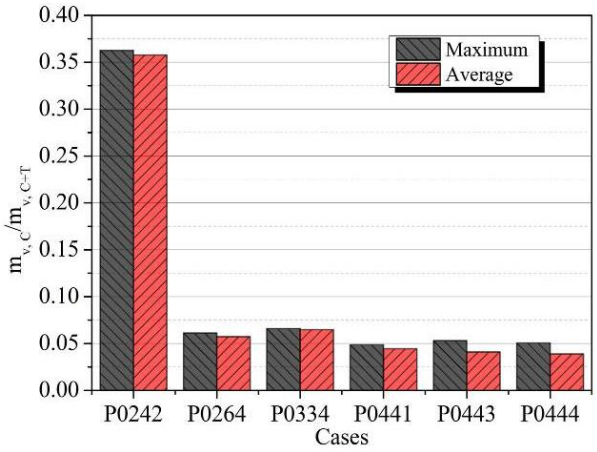

Fig. 7. Mass transfer ratio in various cases.

Table 2. Mass transfer at various air mass fraction and wall sub-cooling conditions

Wa	ΔT	Mc	M_T	Mc + M_T	M_T/(Mc+ M_T)
0.1	10	9.47E-03	-4.90E-05	9.43E-03	0.51%
0.1	60	2.29E-02	3.40E-04	2.32E-02	1.46%
0.1	120	2.61E-02	7.95E-04	2.69E-02	2.96%
0.5	10	2.11E-03	2.39E-05	2.13E-03	1.12%
0.5	60	7.53E-03	2.52E-04	7.78E-03	3.24%
0.5	120	9.25E-03	5.40E-04	9.79E-03	5.52%
0.9	10	3.30E-04	1.82E-05	3.48E-04	5.24%
0.9	50	1.19E-03	4.80E-05	1.24E-03	3.88%
0.9	80	1.50E-03	7.19E-05	1.57E-03	4.57%
0.99	10	4.38E-05	2.41E-06	4.62E-05	5.22%
0.99	20	7.66E-05	3.38E-06	8.00E-05	4.22%
0.99	30	2.55E-04	3.82E-06	2.59E-04	1.48%

The results of superheated group are shown in Fig. 8. It indicates that in the conditions that have large air mass fraction and small wall sub-cooling, the thermal diffusion proportion has an obvious enlargement with the increase of gas superheat. The maximum relative difference is more than 40%.

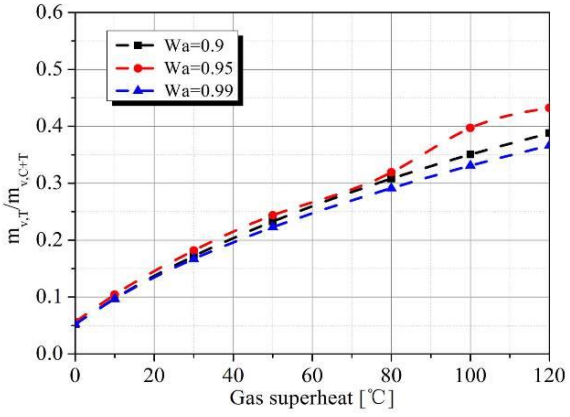

Fig. 8. Mass transfer ratio (ΔT=10℃).

4.2 The diffusion coefficient effect

The constant of proportionally in Fourier's law was defined as the thermal conductivity. Similarly, the constant of proportionality in Fick's law is defined as the binary diffusion coefficient. It means the mass of the substance diffuses through a unit surface in a unit time at a concentration gradient of unity. The theory description in binary gas mixtures at low to moderate pressures has been well developed by Chapman and Enskog independently between 1910 and 1920. The theory results from solving the Boltzmann equation, and the derived equation is given as

$$D = \frac{0.0266T^{3/2}}{PM_{AB}^{1/2}\sigma_{AB}^{2}\Omega_{D}} \ m^2/s \qquad (24)$$

Even though the theoretical equation could provide a reasonable prediction in various conditions, parameters like the molecular collision integral and character length is complicated to evaluate. For the sake of providing a simplified diffusion coefficient equation in engineering applications, Gilliland correlated an equation with new experimental data of various organic vapors at one atmosphere at temperatures from 25.9℃ to 341℃ in 1934. The modified correlation is based on the Maxwell's original equation, and its final form is described as

$$D = \frac{0.04357T^{1.5}\sqrt{\frac{1}{M_A}+\frac{1}{M_B}}}{p\,(V_A^{1/3}+V_B^{1/3})^2} m^2/s \qquad (25)$$

In the subsequent few decades, some other simplified recommended empirical collations for diffusion coefficient are provided, such as the classical Fuller equation in 1966 [18] and the Marrero and Mason equation in 1972 [25]. Similar equation forms with different constants and power exponents are also quoted in the recent condensation numerical simulations. For instance the equation quoted by Yadav [11]. The calculation expressions are given as follows

(1) Fuller

$$D = D_0 (\frac{T}{T_0})^{1.75} (\frac{P}{P_0})^{-1} \tag{26}$$

(2) Marrero and Mason

$$D = 1.87 \times 10^{-5} \frac{T^{2.072}}{P} \tag{27}$$

(3) Yadav quoted

$$D = 4.88 \times 10^{-4} T^{3/2} P^{-1} \tag{28}$$

To evaluate the diffusion coefficient effect in a large parameter scope, cases with various air mass fractions and wall sub-cooling were simulated. The air mass fraction ranges from 0.1 to 0.9, and the wall sub-cooling is between 10 and 40℃. Since the diffusion coefficient is considered to have a negative power relationship with the pressure in all the five equations, the influence of pressure is neglected. The pressure is chosen as 0.2 MPa and the mainstream velocity is 0.5 m/s. The simulated average heat transfer coefficient distribution is shown in Fig. 9. The result indicates that the condensation heat transfer coefficient calculated by various diffusion coefficients demonstrates different distributions. Generally, the maximum relative difference increases with the decrease of air mass fraction with a value between 12% and 26%. The maximum deviation appears at the air mass fraction of 0.1. The comparison between Fig. 9 (a) and Fig. 9 (b) indicates that the wall sub-cooling also has an effect on the maximum relative difference, but it is not as obvious as the air mass fraction.

The local heat flux profiles obtained by various diffusion coefficient expressions at an air mass fraction of 0.1 are shown in Fig. 10. It demonstrates that the heat flux distribution can be mainly classified into two regions, one is the decrease region, and the other is the slow increase region. In addition, the decrease region can be further divided into two sections. One is the fast decrease section, and the other is the low decrease section. The differences among various diffusion coefficient models is large at the fast decrease section. Then, the relative difference is maintained at a relative small value at the slow decrease section, until a further enlarge in the slow increase region.

The above discussions indicates that the application of various diffusion coefficient expressions has influence on the effective evaluation of condensation heat transfer property. Since all of the five expressions have been commonly applied in the previous researches, the reasonable application of a diffusion coefficient model should be specified. The kinetic theory is originally derived from the Boltzmann equation. It has theoretical bases and could give reasonable predictions in various mixture gases, whereas the deviation could be large due to the theoretical assumptions. Gilliland proposed a simplified empirical model in engineering application; however, the equation is correlated by various binary gas mixtures, so the deviation may be large when applying to a specific mixture like steam-air. The Fuller model and Marrero model are updated models with parameters specific for the steam-air mixture and the simulation results by these two models are similar to each other. Thus, the Fuller model and Marrero model are recommended in the steam condensation simulations. To have an insight on this problem, further experimental investigations should be carried out to validate the applicability of the diffusion coefficient calculation models.

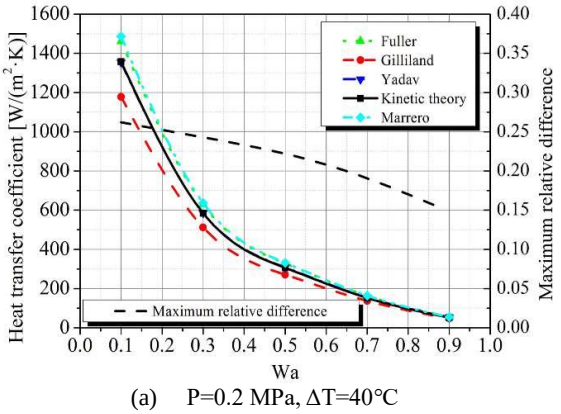

(a) P=0.2 MPa, ΔT=40℃

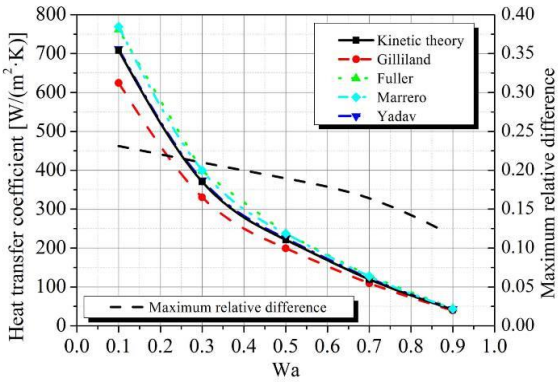

(b) P=0.2 MPa, ΔT=40℃

Fig. 9. Average heat transfer coefficient obtained by various diffusion coefficients.

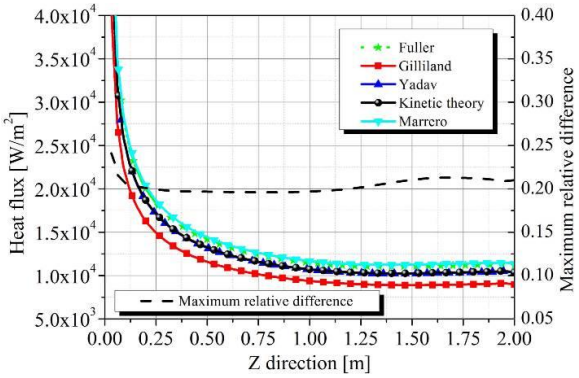

(a) Wa=0.1, ΔT=10

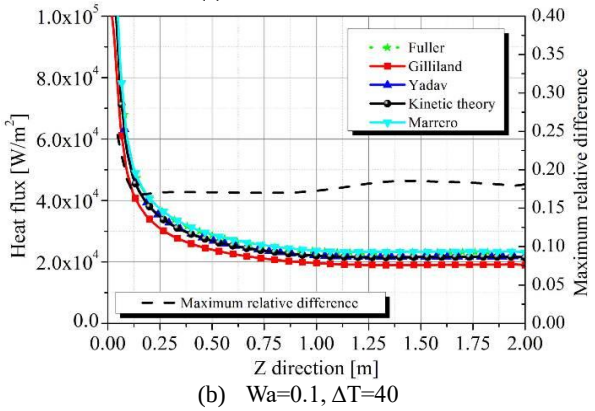

(b) Wa=0.1, ΔT=40

Fig. 10. Local heat flux obtained by various diffusion coefficients.

4.3 The wall treatment effect

To evaluate the wall treatment effect in a large parameter range (*e.g.* velocity, air concentration and pressure), all the six experimental cases listed in Table 1 were considered. In the mesh generation process, the total thickness, increasing ratio and total layers of prism meshes were controlled delicately to ensure the first layer of boundary mesh in within the particular region (viscous sub-layer, buffer layer or log-law layer). The total boundary layer thickness ranges from 0.02 m to 0.06 m, the increasing ratio ranges from 1.1 to 1.4 and the total layer of prism mesh ranges from 2 to 15. The scope of Y+ is between 1 and 191.7. Comparisons of local heat flux, average heat flux and outlet profiles (velocity, temperature and concentration) were made between the numerical results and the experimental ones.

Figures 11-16 show the local and average heat flux on the condensation wall with different Y+ values. Along Z direction, the local heat flux can be classified into two regions. One is the developing region with high heat flux gradient, and the other is the fully developed region with flat heat flux. The large gradient of heat flux in the developing region is caused by the development of the concentration layer of non-condensable gas. The thin layer of air contributes to the high heat flux. Numerical solutions with different Y+ values showed different characters in these two regions.

It is indicated that, the local heat flux in cases with Y+<5 matches well with the experimental results in both developing and fully developed region. In the cases with 5<Y+<30, the local heat flux generally has an over prediction in both the developing and developed region. When Y+>30, the local heat flux has an under prediction in the developing region and has an over prediction in the fully developed region. The maximum deviations of local heat flux in different cases are mostly within 30%.

For the average heat flux, the cases with Y+< 5 and Y+>30 agree well each other, and they match well with the experimental results. It is illustrated that, in the cases have Y+ value in between, the average heat flux firstly increased with the increase of Y+ value and followed by a decrease. They overall have

an over prediction of average heat flux. Among all the numeral cases, the maximum deviation of average heat flux is within 28%.

By comparing the average heat flux of P0441, P0443 and P0444, it demonstrates that the scattering of average heat flux enlarges with the decrease of mainstream velocity. The P0441 case (3 m/s) has the minimum deviation of 6.7%, and the P0444 case has the maximum deviation of 25.6%.

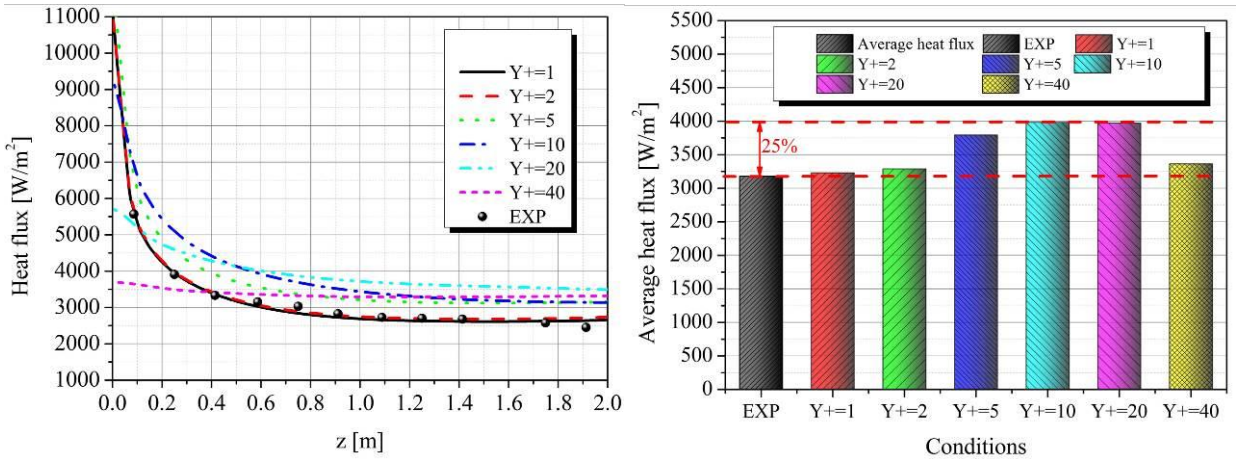

Fig. 11. Local (left) and average (right) heat flux of P0443.

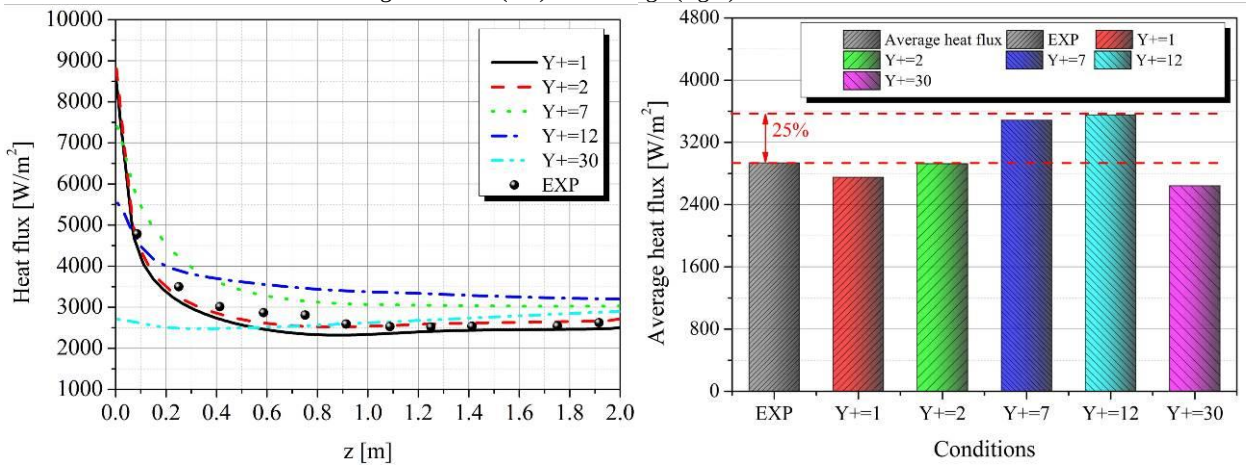

Fig. 12. Local (left) and average (right) heat flux of P0444.

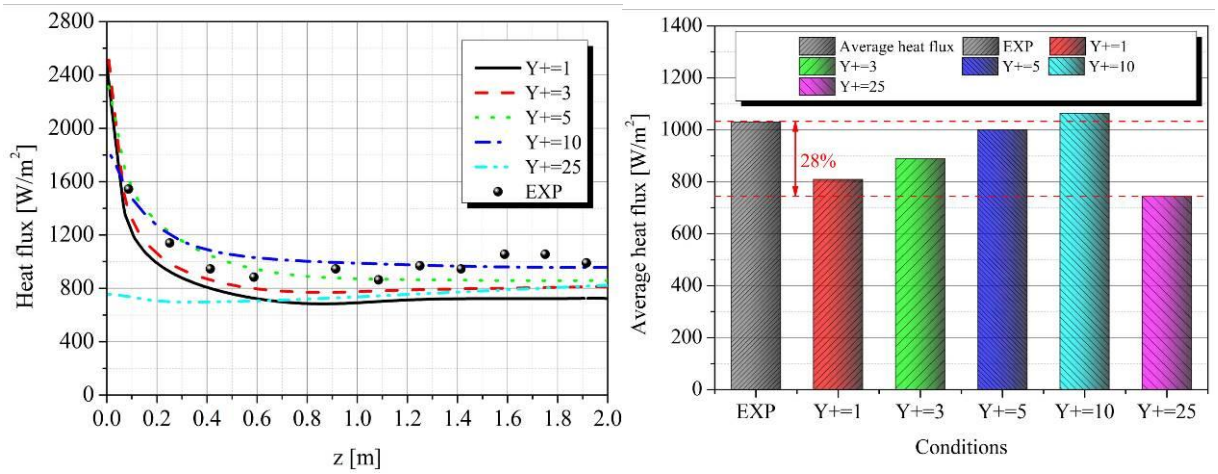

Fig. 13. Local (left) and average (right) heat flux of P0344.

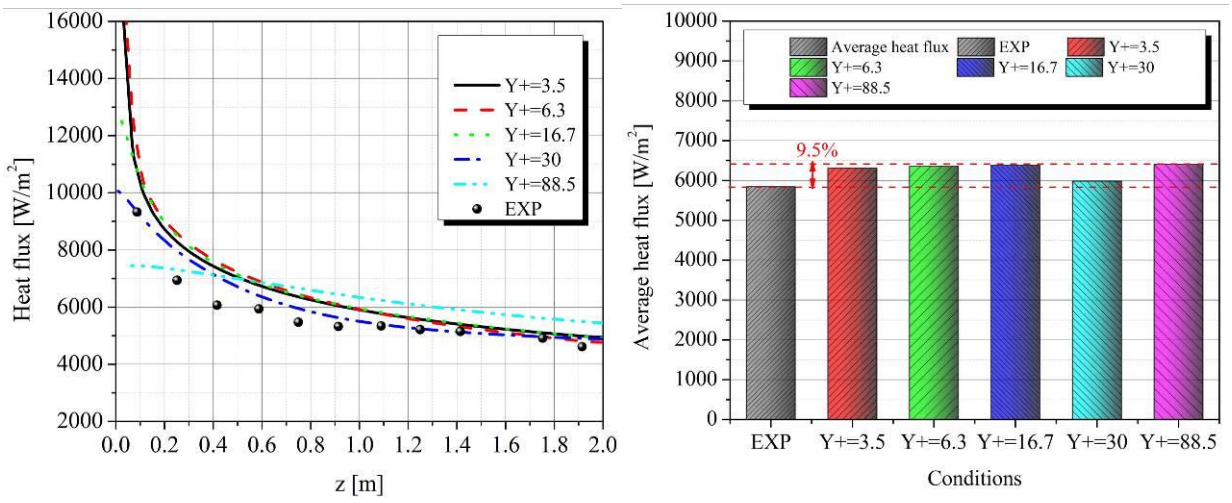

Fig. 14. Local (left) and average (right) heat flux of P0441.

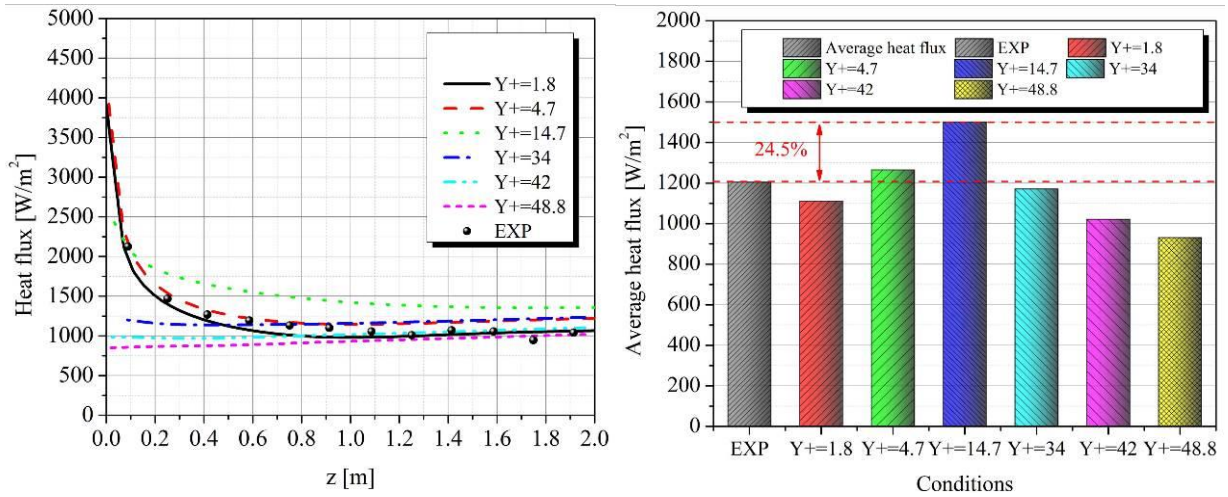

Fig. 15. Local (left) and average (right) heat flux of P0264.

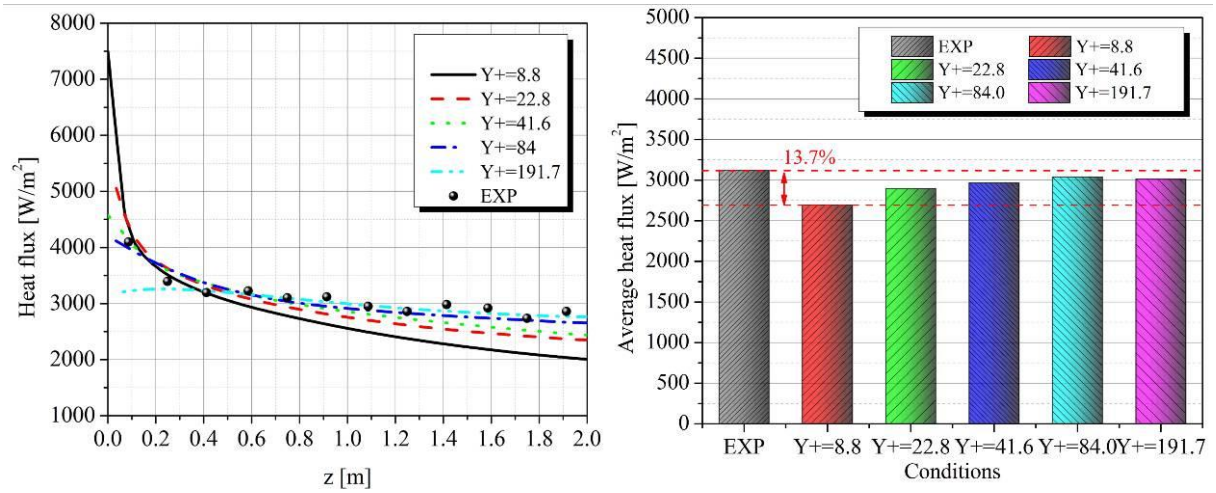

Fig. 16. Local (left) and average (right) heat flux of P0242.

In containment thermal-hydraulic analyses, steam condensation is coupled with other phenomena in the gas region, such as the large space natural convection, temperature/concentration stratification *etc*. For instance, when steam condensates at the liquid-gas interface, a high concentration air layer will be developed in the near wall region. As a consequence, the gas density in the near wall region

is larger than that in the mainstream. The gravity effect will result in a larger velocity profile in the near wall region, and this phenomena will be more obvious at the small mainstream velocity conditions. The change of velocity profile may further influence the temperature and concentration distribution. Thus, the effect of wall treatment on these phenomena should also be evaluated. For this purpose, the outlet profile of velocity, temperature and concentration are evaluated by comparing the cases with Y+ values in the three different regions (viscous sub-layer, buffer layer and log-law layer). The experimental cases of P0441, P0443 and P0444 are selected to cover different mainstream velocities.

Fig. 17 shows the outlet velocity profiles of different cases. It is indicated that when the inlet velocity is less than 1 m/s, the near-wall accelerate effect becomes obvious. This is due to the high density gas (caused by the low temperature and high air concentration) in the near wall region accelerated the gas flow by the buoyancy effect. In contrast, the acceleration effect is not obvious at an inlet velocity of 3 m/s. In case P0444, the near wall velocity (1 m/s) is twice of the inlet velocity (0.5 m/s). Here, we assume the cases with Y+< 5 could give a good prediction of the local phenomena (refined grids were used). The cases of Y+>30 and in between are compared and discussed. The results indicated that when the first layer of boundary mesh is in the buffer layer (5<Y+<12), the outlet velocity is similar with the Y+<5 cases. However, in the cases with Y+>30, there is an under prediction of outlet velocity.

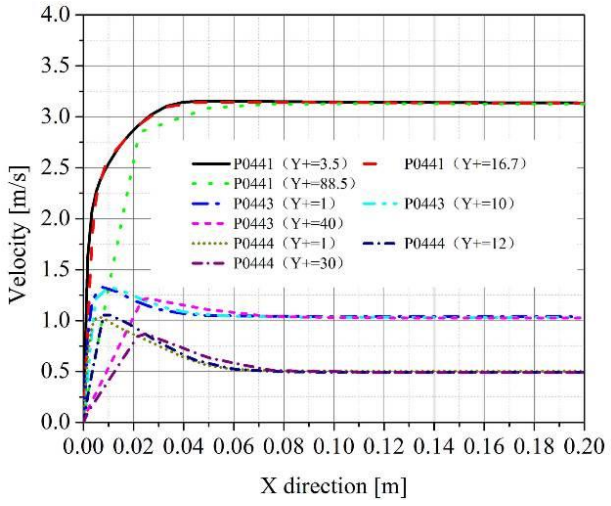

Fig. 17. Velocity distribution at outlet.

Figure 18 shows the comparison of outlet temperature profiles. It is indicated that the largest temperature gradient is within the 0.06 m thickness close to the condensation wall. For the cases with Y+<5 and 5<Y+<30, the temperature profiles agree well with each other. In the cases with Y+>30, the temperature profile is generally under predicted. Fig. 19 shows the concentration profile at the outlet. Similarly, both the Y+<5 and 5<Y+<30 cases could give a good prediction of the large concentration gradient in the developing region. The cases with Y+>30 have under predictions of air concentration in the near wall region.

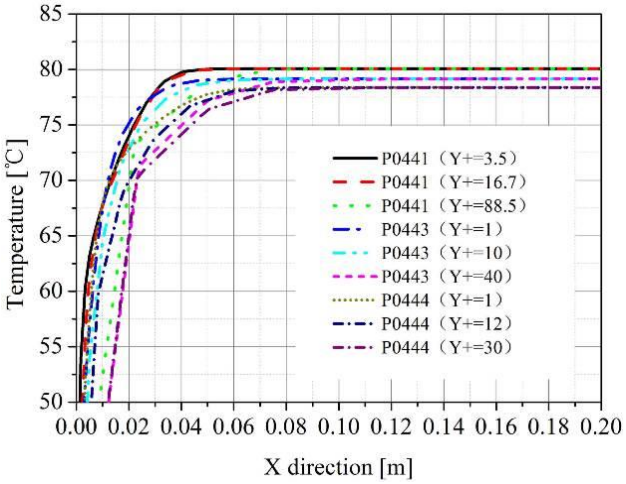

Fig. 18. Temperature distribution at outlet.

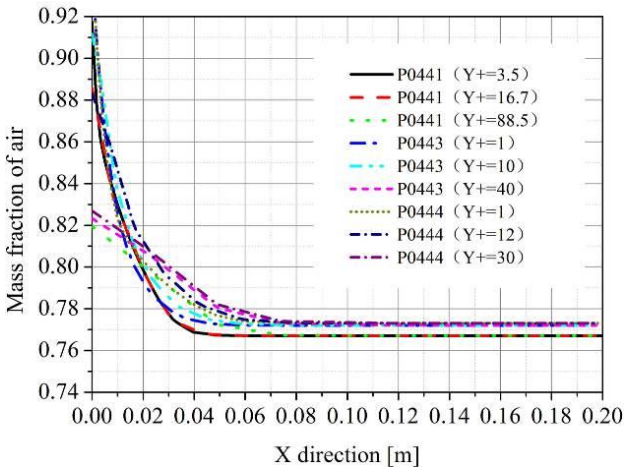

Fig. 19. Concentration distribution at outlet.

5 Conclusions

To evaluate the effect of influencing parameters on steam condensation heat transfer property, the Soret effect, diffusion coefficient effect and wall treatment effect are evaluated separately. The conclusions are

given as follows:

For the soret effect. The proportion of thermal diffusion induced mass transfer is mainly related to two factors. One is the air mass fraction, the other is the wall sub-cooling. The saturation group results indicate that the thermal diffusion induced mass transfer only takes a small part in the total mass transfer, and the proportion is generally within 5%. The superheated group result shows that in the conditions with large air mass fraction and small wall sub-cooling, the thermal diffusion has an obvious increase with the increase of gas superheat. The maximum relative difference is more than 40%.

For the diffusion coefficient effect. The diffusion coefficients predicted by the theoretical expression and some empirical correlations are compared. It has been concluded that the average condensation heat transfer coefficient calculated by various diffusion coefficients demonstrates different distributions. Generally, the maximum relative difference increases with the decrease of air mass fraction with a value between 12% and 26%. The wall sub-cooling also has an effect on the maximum relative difference, but it is not as obvious as the air mass fraction. For the local heat flux property, the differences among various diffusion coefficient models is large at the fast decrease section. Then, the relative difference is maintained at a relative small value at the slow decrease section, until a further enlarge in the slow increase region. The Fuller and Marrero model are recommended in the steam condensation evaluations, yet the diffusion coefficient model still needs broader experimental validations.

To evaluate the wall treatment effect, the boundary layer mesh was controlled exquisitely to ensure the first layer is located in the specific layers (viscous sub-layer, buffer layer and log-law layer). The results showed that in the cases with Y+<5, the predicted local heat flux matches well with the experimental results in the developing region and fully developed region. In the cases with 5<Y+ <30, the local heat flux generally has an over prediction in both the developing and developed region. When Y+>30, the local heat flux has an under prediction in the developing region and has an over prediction in the fully developed region. The maximum deviations of local heat flux in different cases are mostly within 30%. For the average heat flux, the cases with Y+< 5 and Y+>30 agree well each other, and they match well with the experimental results. In the cases with 5<Y+<30, the scattering of average heat flux increases with the decrease of mainstream velocity. Both the case with Y<5 and 5<Y+<30 could give a reasonable prediction of local field profile, whereas the Y+>30 cases have an under prediction of local profiles.

Nomenclature

General notation

B	Bird Suction parameter
C_1, C_2, $C_{\varepsilon 1}$, $C_{\varepsilon 3}$,	constants
D_{eff}	corrected mass diffusion coefficient, m^2/s
D	diffusion coefficient, m^2/s
D_0	mass diffusion coefficient under the standard state, m^2/s
D_T	thermal diffusion coefficient, m^2/s
E	energy, J
EXP	experiment
f	body force, N/m^3
h	heat transfer coefficient, $W/(m^2 K)$
G_b	generation of turbulence kinetic energy due to mean buoyancy, m^2/s^2
k	turbulent kinetic energy, (m^2/s^2)
k	Boltzmann's constant, 1.3806503×10^{-23}, J/K
k_{eff}	effective thermal conductivity, $W/(m K)$
m	mass flux, $kg/(m^2 s)$
M	molar weight, g/mol
n	normal direction to the condensation wall
P	pressure, Pa
P_0	pressure under standard conditions. Pa
P	surface force, N/m^2
P_k	generation of turbulence kinetic energy due to mean velocity gradients, m^2/s^2
Pr	Prandtl number
q	surface heat flux, W/m^2
$\bar{S}$	mean strain rate tensor
S_h	energy source, $J/(m^3 s)$
S_m	mass source, $kg/(m^3 s)$
$S_{\rho v}$	momentum source, N/m^3
SIM	simulation
T	temperature, K
t	time, s

T_0 temperature under standard conditions, K
μ^* reduced dipole moment, debyes
w velocity, m/s
x length, m
X mole fraction
Y_M turbulence dissipation rate contributed by fluctuating dilatation, m^2/s^3

Greek letters

δ reduced dipole moment, debyes
ω mass fraction
Ω diffusion collision integral, dimensionless
ε turbulence dissipate rate, m^2/s^3
ε Lennard-Jones energy, kJ/mol
ζ orientation equation
σ characteristic length, $\dot{A}$
ν kinematic viscosity, m^2/s
Δ Thickness of the cells close to condensation wall, m
ρ density, kg/m^3
μ dynamic viscosity, Pa s
θ_B logarithmic correction factor

Subscripts

a air
cond condensation
i interface
j species/rectangular coordinate axes
k turbulence kinetic energy
sat saturation
t turbulence
v vapor
w wall
ε turbulence dissipation

References

[1] PACI, S., and FORGIONE, N.: Computational analysis of vapour condensation in presence of air in the TOSQAN Facility, International Journal of Heat and Technology, 26 (2005) 1-14.

[2] DE lA ROSA, J.C., ESCRIVA, A., HERRANZ, L.E., CICERO, T., and MUNOZ-COBO, J.L.: Review on condensation on the containment structures, Progress in Nuclear Energy, 51(1) (2009) 32-66.

[3] DEHBI, A., GOLAY, M.W., and KAZIMI, M.S.: Condensation experiments in steam-air and steam-air-helium mixtures under turbulent natural convection, in: International Heat Tranfer, AIChe, Minneapolis, 1991, pp. 19-28.

[4] PARK, S.K., KIM, M.H., and YOO, K.J.: Condensation of pure steam and steam-air mixture surface waves of condensate film on a vertical wall, International Journal of Multiphase Flow, 22 (1996) 893-908.

[5] TONG, P., FAN, G., SUN, Z., and DING, M.: Experimental study of steam–air condensation over a vertically longitudinal finned tube, International Journal of Heat and Mass Transfer, 89 (2015) 1230-1238.

[6] SPARROW, E.M., and LIN, S.H.: Condensation Heat Transfer in the Presence of a Noncondensable Gas, Journal of Heat Transfer, 86(3) (1964) 430-436.

[7] PETERSON, P.F., SCHROCK, V.E., and KAGEYAMA, T.: Diffusion Layer Theory for Turbulent Vapor Condensation With Noncondensable Gases, Journal of Heat Transfer, 115(4) (1993) 998-1003.

[8] SHANG, D.Y., and ZHONG, L.C.: Extensive study on laminar free film condensation from vapor–gas mixture, International Journal of Heat and Mass Transfer, 51(17) (2008) 4300-4314.

[9] MARTIN-VALDEPENAS, J.M., JIMENEZ, M.A., MARTIN-FUERTES, F., and BENITEZ, J.A.F.: Comparison of film condensation models in presence of non-condensable gases implemented in a CFD Code, Heat and Mass Transfer, 41(11) (2005) 961-976.

[10] BIAN, H., SUN, Z., DING, M., ZHANG, N., and MENG, Z.: Application and evaluation of automatic wall treatment on diffusion boundary layer based steam condensation model in presence of air, in: International Topical Meeting on Nuclear Reactor Thermal Hydraulics, Xi'an China, 2017.

[11] YADAV, M.K., KHANDEKAR, S., and SHARMA, P.K.: An integrated approach to steam condensation studies inside reactor containments: A review, Nuclear Engineering and Design, 300 (2016) 181-209.

[12] ROYL, P., ROCHHOLZ, H., BREITUNG, W., TRAVIS, J., and NECKER, G.: Analysis of steam and hydrogen distributions with PAR mitigation in NPP containments, Nuclear Engineering and Design, 202(2) (2000) 231-248.

[13] GILLILAND, E.R.: Diffusion Coefficients in Gaseous Systems, Ind. Eng. Chem, 26 (1934) 681-685.

[14] KO, M.S., KIM, S., and JERNG, D.W. Development of A CFD Modle for condensation of steam-air mixture at the exterior surface of a circular tube, in: 23rd International Conference on Nuclear Egnineering, Chiba, Japan, 2015.

[15] FU, W., LI, X., WU, X., and CORRADINI, M.L.: Numerical investigation of convective condensation with the presence of non-condensable gases in a vertical tube, Nuclear Engineering and Design, 297 (2016) 197-207.

[16] MIMOUNI, S., FOISSAC, A., and LAVIEVILLE, J.: CFD modelling of wall steam condensation by a two-phase flow approach, Nuclear Engineering and Design, 241(11) (2011) 4445-4455.

[17] DEHBI, A., JANASZ, F., and BELL, B.: Prediction of steam condensation in the presence of noncondensable gases using a CFD-based approach, Nuclear Engineering and Design, 258 (2013) 199-210.

[18] BEJAN, A.: Convection heat transfer fourth edition, John Wiley & Sons, New Jersey, 2013.

[19] CHENG, X., BAZIN, P., CORNET, P., HITTNER, D., and JACKSON, J.D.: Experimental data base for containment thermalhydraulic analysis, Nuclear Engineering and Design, 204 (2001) 267-284.

[20] BIRD, R.B., STEWARD, W.E., and LIGHTFOOT, E.N.: Transport Phenomena, John Wiley & Sons, 28(2) (2002) 338–359.

[21] LANDAU, L.D., LIFSHITZ, E.M., and FLUID Mechanics: Landau and Lifshitz: Course of Theoretical Physics, 2013.

[22] STAR-CCM+ documentation, (version 10.02, 2015).

[23] KEE, R.J., DIXON-LEWIS, G., WARNATZ, J., COLTRIN, M.E., and MILLER, J.A.: A Fortran Computer Code Package For The Evaluation Of Gas-Phase, Multicomponent Transport Properties, Lewis, (1986).

[24] MONCHICK, L., and MASON, E.A.: Transport Properties of Polar Gases, Journal of Chemical Physics, 35(5) (1961) 1676-1697.

[25] CENGEL, Y.A.: Heat and mass transfer: a practical approach, Tata McGraw-Hill education, 2006.